A Passive Negative Magnetic Reluctance Structure-Based kHz Transformer for Improved DC Magnetic Bias Withstanding

Yuanxi Chen, Weinong Fu, Hongjian Lin, *Member, IEEE*, and Shuangxia Niu, *Senior Member, IEEE*

***Abstract*—How to effectively withstand the dc magnetic bias is one of the key aspects of transformer design. General approaches either require additional active power electronics devices or apply complicated control strategies, causing the increased cost or reduced reliability. In this article, a passive negative magnetic reluctance structure (NMRS) is proposed and installed in the air gap of the open-core transformer, which could achieve improved dc magnetic bias withstanding capability without extra active devices. The key criterion of the proposed design is to employ the NMRS with a frequency-variation magnetic reluctance property as a magnetic bandpass filter, which shows a negative equivalent magnetic reluctance for the fundamental component of flux. Nevertheless, it presents a high magnetic reluctance for the dc component. With the proposed design, the transformer provides a strong withstanding dc bias capability and a low magnetizing current as well as high efficiency. Accordingly, both the advantages of open-core and closed-core transformers could be obtained with the proposed design. For verification, a 500-W EE55-based core prototype is constructed and verified with sinusoidal and square wave excitation. Electromagnetic analysis and experimental results are provided to demonstrate the effectiveness of the proposed design.**

***Index Terms*—DC bias withstanding capability, magnetic bandpass filter, negative magnetic reluctance, transformer.**

I. Introduction

KILOHERTZ (kHz) transformer is a key device widely applied in switching power supply [1], [2] and isolated converters [3], [4], [5], [6]. Its main role is to isolate the primary and secondary circuits. The key merits of the kHz transformer are small volume, low magnetic hysteresis loss, high efficiency, and lightweight [7], [8], [9], [10]. However, the dc bias problem of the kHz transformer seriously restricts the performance of the isolated converters. Based on the voltage on the primary side of the transformer, the isolated converters are mainly classified as dual active bridge (DAB) converters with a square wave excitation transformer [11], [12], [13], [14] and matrix ac–dc/ac–ac converters with a sinusoidal excitation transformer [15], [16]. This is because the dc bias saturates the flux in the magnetic core and reduces the output voltage of the transformer. In applications with both sinusoidal and square wave excitation, dc bias is always generated by an asymmetrical input voltage, which is hard to be eliminated. To withstand the dc bias, the open-core structure is used for its high magnetic reluctance and less sensitivity to dc flux bias. However, high magnetic reluctance results in a relatively high magnetizing current, low efficiency, and low power factor. Hence, how to provide a strong withstand dc bias capability while maintaining a relatively low magnetic reluctance is the key to developing a high-efficiency transformer.

Many research works have been carried out in terms of the dc bias issue of the transformer, including the dc bias detection, measurement, prediction, and suppression [17], [18], [19], [20], [21], [22], [23], [24], [25], [26], [27], [28]. Based on the design mechanism, general dc bias suppression methods can be divided into two categories, namely power electronics converter design and magnetic core design. The former includes the control strategy and converter topology design, whereas the latter is focused on magnetic core topology and material design [22], [23], [24], [25].

For the converter-based solutions, an auxiliary winding is added and used to compensate for the dc magnetic bias by generating a revised modulation flux [22]. A decoupling control method is proposed for eliminating the dc bias, which can compensate for the bias within 30 ms at the operating frequency of 1 kHz [23]. A flux balancing control technology of the transformer applied to the DAB converter is proposed to make the transformer operate normally with a 0.1-A dc bias [26]. A gravitational search algorithm-based switching combination scheme is proposed to improve the efficiency of the dc blocking devices and the transformer [27].

For the magnetic core-based solution, the auxiliary core and winding are added and the high-frequency signals are injected to improve the withstand dc bias capability [24]. A nanocomposite magnetic material is utilized as the magnetic core to improve the withstanding dc bias capability [25]. Yao et al. [28] proposed

Manuscript received 4 May 2022; revised 14 July 2022; accepted 19 August 2022. Date of publication 29 August 2022; date of current version 10 October 2022. This work was supported by the Research Grant Council of the Hong Kong SAR Government under Project PolyU152180/19E and Project PolyU152185/18E. Recommended for publication by Associate Editor M. Hartmann. *(Corresponding authors: Weinong Fu; Shuangxia Niu.)*

Yuanxi Chen, Hongjian Lin, and Shuangxia Niu are with the Department of Electrical Engineering, The Hong Kong Polytechnic University, Hong Kong, SAR China (e-mail: 19109864r@connect.polyu.hk; hongjian.lin@polyu.edu.hk; eesxniu@polyu.edu.hk).

Weinong Fu is with the Shenzhen Institutes of Advanced Technology, Chinese Academy of Sciences, Shenzhen 518038, China (e-mail: wn.fu@siat.ac.cn).

Color versions of one or more figures in this article are available at https://doi.org/10.1109/TPEL.2022.3202038.

Digital Object Identifier 10.1109/TPEL.2022.3202038

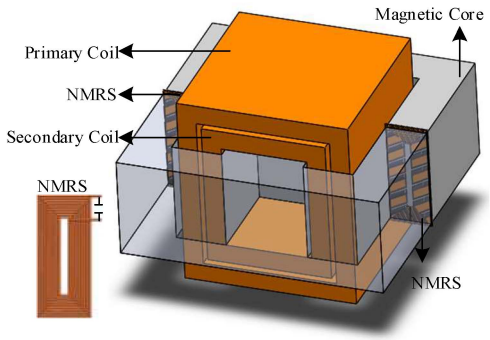

Fig. 1. Configuration of the NMRS-based transformer.

a geometric variables optimization method for transformers applied to DAB.

However, the converter-based solutions require additional active power electronics devices and relevant control strategies to withstand the dc bias. The magnetic core-based solution still requires extra core structure and control strategies, bringing extra weight and increased cost issues.

To solve the aforementioned issues, in this article, a passive negative magnetic reluctance structure (NMRS) is proposed, which is installed in the air gap of the open-core transformer and requires no additional control strategies, power electronics devices, and uncommon material. The proposed NMRS can be esteemed as a copper-based magnetic bandpass filter, in which only the flux at the selected frequency can be enhanced. For the dc component and high order harmonics of the flux, NMRS represents a high magnetic reluctance as air. But for the magnetic field at the selected frequency, the NMRS shows a negative equivalent magnetic reluctance. Therefore, the bias caused by the dc component can be suppressed significantly, which makes the NMRS-based transformer inherently have the advantages of low magnetizing current, high efficiency, and strong withstand dc bias capability.

In this article, the theoretical analysis and mathematical model of the proposed NMRS are given, including the frequency-variation property on magnetic reluctance and negative magnetic reluctance region design. The magnetic circuit analysis of the transformer with and without the proposed NMRS is compared, theoretically demonstrating how the NMRS-based transformer achieves both high efficiency and strong withstand dc bias capability. The key properties of the NMRS-based transformer, including withstanding dc bias capability, high efficiency, and low magnetizing current, are verified via experiments.

II. Theoretical Analysis of the NMRS-Based Transformer

A. Structure Configuration and Analysis

The overall configuration of the NMRS-based transformer with an EE55 core is shown in Fig. 1. Considering the windings installing issue of the transformer, the air gaps are designed at the side poles and the NMRS is installed in the corresponding two air gaps.

TABLE I
Parameters of the NMRS-Based Transformer

Symbol	Quantity	Value
A_p	area product (cm^4)	13.6764
A_e	effective magnetic cross area (mm^2)	354
A_w	core winding window area (mm^2)	386.34
A_L	inductive factor (nL/N^2)	7100
V_e	effective volume (mm^3)	43700
A	core width (mm)	55.15
B	half core length (mm)	27.5
C	core depth (mm)	20.7
D	middle pole width (mm)	17.2
E	side pole inner width (mm)	37.5
F	half pole length (mm)	18.5
d_{gap}	air gap length (mm)	0.6
f	operating frequency (kHz)	55
U_{in}	input voltage (V)	90
N_p	number of turns of primary coil	20
N_s	number of turns of secondary coil	20

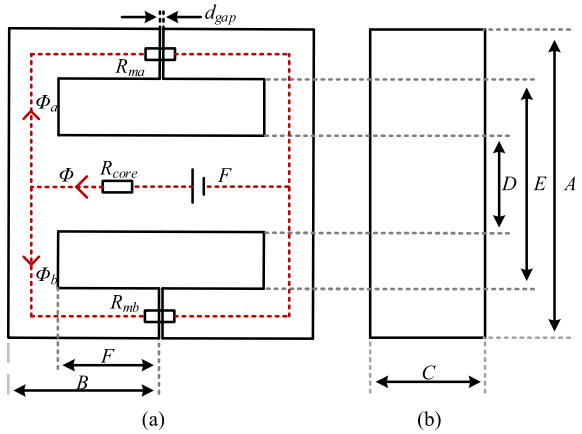

Fig. 2. Diagrammatic drawing of the magnetic core and corresponding magnetic circuit. (a) Front view and equivalent magnetic circuit. (b) Top view.

The detailed geometric parameters of the magnetic core and corresponding diagrammatic drawing are shown in Table I and Fig. 2, respectively. The material of the magnetic core is selected as the PC44 with a maximum magnetic flux density of 0.4 T. The NMRS is made of copper wire with a width of 0.6 mm.

All the transformers, including the proposed structure, are designed following the basic operating rule.

$$U_{\text{inmax}} = 4fNB_{\text{max}}A_e \tag{1}$$

where U_{inmax}, f, B_{max}, N, and A_e are the maximum input voltage, operating frequency, the maximum magnetic induction intensity of core material, turns of the primary coil, and effective magnetic cross area, respectively.

The equivalent magnetic circuit of the NMRS-based transformer is shown in Fig. 2(a), in which the F, R_{core}, and ϕ are the magnetomotive force generated by the primary coil, magnetic reluctance of magnetic core, and the main flux. ϕ_a and ϕ_b are the fluxes and R_{ma} and R_{mb} the magnetic reluctance of NMRS or air gap of branches, respectively, depending on the transformer topology.

The magnet circuit equation of the NMRS-based transformer is represented as follows:

$$\phi_{\text{NMRS}}(\omega t) = \frac{F(\omega t)}{R_{\text{core}}+R_{ma}(\omega t)//R_{mb}(\omega t)} \tag{2}$$

where $\phi_{\text{NMRS}}(\omega t)$ is the flux in the magnetic core of the NMRS-based structure.

The flux ϕ of the transformer is shown as follows:

$$\phi = \frac{F}{R_m} = \frac{Ni}{R_m} \tag{3}$$

where N and i are the numbers of turns of the primary coil and the current through it. For the general structures, the magnetic reluctance R_m is fixed, which will not be affected by frequency variation. Hence, the magnitude–frequency characteristic of the magnetic reluctance is always ignored.

The magnetic reluctance of the NMRS structure considering frequency variation is expressed as

$$R_{ma} = R_{mb} = R_0 + R_1 \sin(\omega t) + \cdots + R_n \sin(n\omega t) \tag{4}$$

where R_0, R_1, and R_n is the magnetic reluctance of the dc component, fundamental wave (rated operating frequency of the transformer), and nth harmonics. Besides, *n* is the order of harmonics.

Different from the air and the PC44 material, the magnetic reluctance of the NMRS is varied with frequency. Hence, if R_1 is designed to be negative and R_0 is keeping positive, the fundamental flux can be improved even with the air gap. Correspondingly, the flux related to the dc component will be decreased sharply.

Based on the above equations, the impact of the flux ϕ on magnetic induction intensity B of the closed-core, open-core, and NMRS-based structures is expressed as follows:

$$B_c = \frac{\phi(\omega t)}{S} = \frac{F}{SR_{\text{core}}} = \frac{Ni}{SR_{\text{core}}} \tag{5}$$

$$B_o = \frac{Ni}{S(R_{\text{core}}+0.5R_{\text{air}})} \tag{6}$$

$$B_{\text{NMRS}} = \frac{Ni}{S(R_{\text{core}}+0.5(R_0+R_1(\omega t)+\cdots R_n(\omega nt)))} \quad (n = 0, 1, \ldots, n) \tag{7}$$

where *S* is the magnetic cross area. B_c, B_o, and B_{NMRS} are the magnetic induction intensity in cores of closed-core, open-core, and NMRS-based structures. R_{core}, R_{airgap}, and $R_0 \sim R_n$ are the magnetic reluctances of the core, air gap, and NMRS.

As shown in (5) and (6), with the same magnetic induction intensity, the magnetic cross area, and the number of turns, the closed-core transformer requires a lower magnetizing current to generate the same magnetic induction intensity B than the open-core transformer, for it has no magnetic reluctance of air gap R_{air}. Hence, compared to the open-core structure, the dc bias current in the closed-core structure will generate a larger bias magnetic induction intensity B , which leads to a weak withstand dc bias capability. Conversely, the open-core structure is less susceptible to dc bias but needs a larger magnetizing current to generate the required magnetic flux with a larger magnetic reluctance.

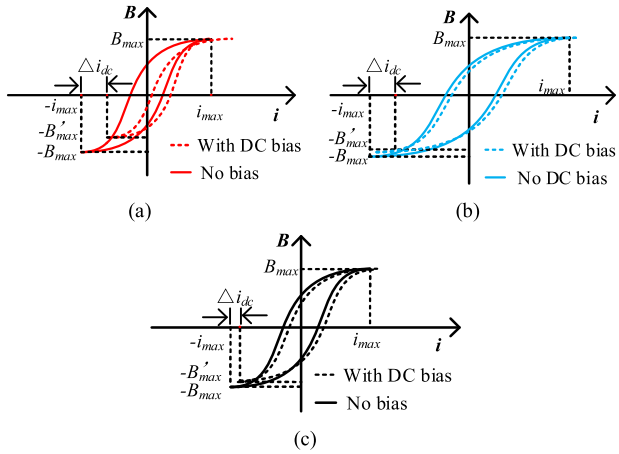

Fig. 3. Equivalent *B–H* curve of transformers. (a) Closed-core structure. (b) Open-core structure. (c) Proposed NMRS-based structure.

Following (7), the frequency-variation property of the NMRS on magnetic reluctance can effectively solve those issues mentioned before. Due to the existence of high dc magnetic reluctance R_0, the impact of dc bias current on magnetic induction intensity B will be weakened. Besides, the magnetic reluctance R_1 at the rated frequency (55 kHz) is designed as negative, which allows a very small magnetizing current to generate a required flux and magnetic induction intensity B. The property of the NMRS is fixed with its inductance and compensation capacitor. The variable of the NMRS-based transformer is the operating frequency that determines the magnetic reluctance of the NMRS.

To intuitively illustrate the effectiveness of the proposed NMRS, the *B–i* relationship of those three structures is given in Fig. 3. Those three structures are assumed to have the same dc bias current $\triangle i_{\text{dc}}$. Its impact on the magnetic induction intensity B is shown as the dashed line in Fig. 3. B of the closed-core reaches its peak at a relevant low magnetizing current $i(\omega t)$, hence, the same dc bias will lead to serious distortion. The *B–i* curve of the open-core structure indicates that it is slightly impacted by the dc bias, however, it needs a larger magnetizing current i to obtain the desired flux and the B, which negatively impacts the efficiency.

The *B–i* relationship of the proposed structure shown in Fig. 3(c) indicates the effectiveness of the NMRS. The abscissa in Fig. 3 is the root-mean-square value of the input current, including the dc, fundamental, and harmonic components. The proposed structure requires a lower magnetizing current to generate the required magnetic intensity B while less is less susceptible to the same $\triangle i_{\text{dc}}$.

B. Negative Magnetic Reluctance Structure (NMRS) Design

The NMRS can be regarded as a low-frequency metamaterial [29], [30], [31], [32], [33], [34], [35], which shows a negative equivalent magnetic reluctance at a selected frequency range. The property of the NMRS can be analyzed via the *L/C* model [36], which is deduced from the permeability. The relationship between magnetic reluctance and permeability is expressed as

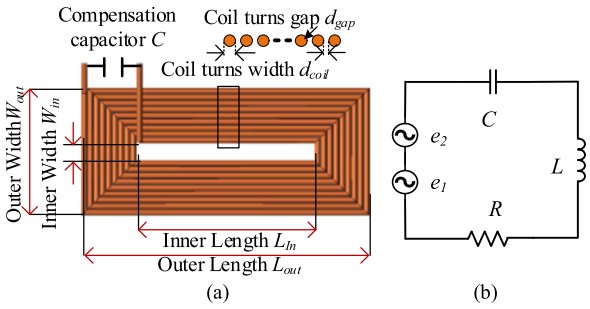

Fig. 4. Negative equivalent magnetic reluctance structure. (a) Overall structure and geometrical parameters. (b) Equivalent circuit.

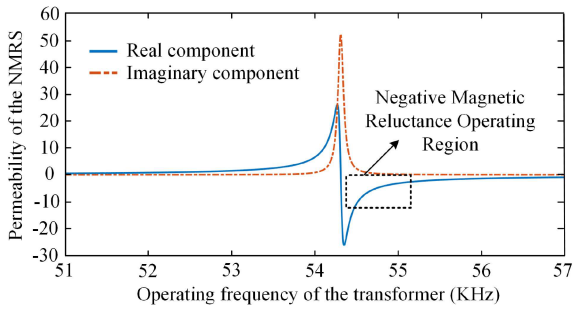

Fig. 5. Relationships between relative permeability and operating frequency.

TABLE II
PARAMETERS OF THE PROPOSED NMRS

Symbol	Quantity	Value
L_{out}	outer length (mm)	20.7
L_{In}	inner length (mm)	7.5
W_{out}	outer width (mm)	8.88
W_{in}	inner width (mm)	0.2
d_{gap}	coil turns gap (mm)	0.45
d_{coil}	coil diameter (mm)	0.55
N	number of turns	10
C	compensation capacitor (uF)	0.45

follows:

$$R_m = \frac{l}{\mu_0 \mu_r A} = \frac{l}{\mu A} \tag{8}$$

where R_m, A, and l are the magnetic reluctance, cross-area, and length of the magnetic core. μ, μ_0, and μ_r are the overall, vacuum, and relative permeability of the NMRS.

Following (8), the negative equivalent magnetic reluctance is obtained when μ_r is negative.

The geometric parameters of the NMRS are shown in Fig. 4 and Table II. The equivalent circuit of the NMRS is shown in Fig. 4(b), where e_1 and e_2 are the voltage induced by the primary coil and secondary coil, respectively. *R*, *L*, and *C* are the internal resistance, equivalent inductance, and compensation capacitor, respectively.

The relationships between the parameters of the NMRS and its permeability can be derived as follows [36].

The equivalent circuit of the NMRS composed of an equivalent resistor *R*, inductance *L*, and the compensation capacitor *C* is shown in Fig. 4(b). Kirchhoff's voltage equation of the NMRS is obtained as follows:

$$I\left(R + \frac{1}{j\omega C} + j\omega L\right) = N\frac{d\phi}{dt} = \frac{dB}{dt}\sum_{k=1}^{N=10} s_k \tag{9}$$

where S_k is the area surrounded by each coil turns, and ϕ is the flux in the NMRS.

The relationship between magnetization intensity M_{NMRS}, volume magnetic susceptibility X_v, and current I is as follows:

$$M_{\text{NMRS}} = \frac{I\sum_{k=1}^{N=10} S_k}{V} \quad e_m = X_v H = X_v \frac{B}{\mu_0 \mu_r} \tag{10}$$

where *V* is the volume of the NMRS, e_m is the magnetic dipole moment, and H is the magnetic field intensity.

Based on (10), the volume magnetic susceptibility X_v is directly related to the relative permeability μ_r of the NMER structure, which is shown as follows:

$$\mu_r = \mu_0 \left(1 + \chi_v\right). \tag{11}$$

Substituting (9) and (10) into (11), the relative permeability of the NMRS can be expressed as

$$\mu_r = 1 + \frac{\mu_0}{lV}\frac{\omega^2}{\omega_0^2 - \omega^2 + j\frac{R\omega}{L}}\sum_{k=1}^{N=10} s_k^2 \tag{12}$$

where l is the length of the magnetic circuit consisting of the NMRS and the air gap of the transformer. ω_0 and ω are the resonant frequency of the NMRS and the operating frequency of the transformer. ω_0 equals $1/\sqrt{LC}$.

According to (12), the relationship between permeability and the operating frequency is shown in Fig. 5. The real component of the permeability represents the magnetic reluctance while the imaginary component is about the loss. Hence, by regulating the *L*/*C* of the NMRS, the magnetic reluctance will represent negative under the operating frequency of the transformer. Besides, the magnetic reluctance of NMRS will be positive beyond the negative magnetic reluctance region. Hence, the NMRS can inherently suppress the dc bias of the transformer.

Based on the abovementioned analysis, the effects of the NMRS on flux in the magnetic core are shown in Fig. 6, where $A_n$is larger than A'_n. Assuming the excitation of those three transformers is the same, the NMRS-based transformer can effectively suppress the dc bias of flux, which is shown in Fig. 6(c).

The design rule of the NMRS is concluded as two steps. The first step is to increase the inductance *L* of the NMRS. The quality factor *Q* of a series *RLC* circuit is proportional to the inductance, which is expressed by follows:

$$Q = \frac{1}{R}\sqrt{\frac{L}{C}} = \frac{\text{stored energy}}{\text{loss}}. \tag{13}$$

The quality factor *Q* is also used to describe the proportion between the stored energy and the loss of the *RLC* circuit. A high-quality factor *Q* will bring the NMRS a high efficiency and performance. The second step of the NMRS design is to reduce the resistor *R*, which is achieved by increasing the sectional area of the coil for NMRS. In addition, the ends of the coil should pass over the NMRS to connect the compensation capacitor *C*. Hence, a thin slot was made in the magnetic core to install the

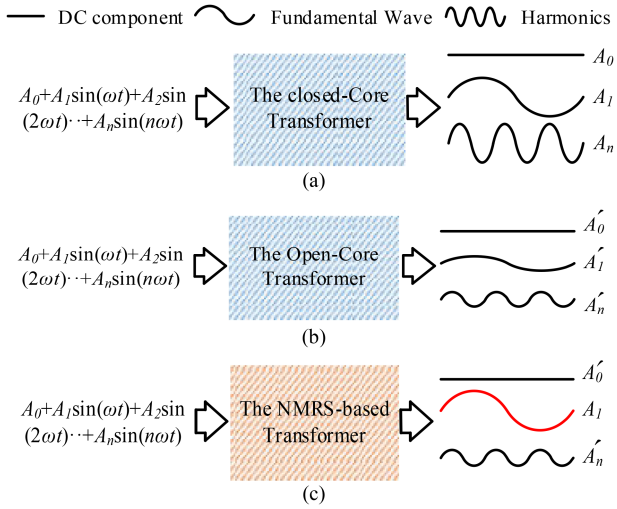

Fig. 6. Effect of different transformer structures on flux in the magnetic core. (a) Closed-core transformer. (b) Open-core transformer. (c) NMRS-based transformer.

intersection part of the NMRS coil, which is shown in Fig. 9(b) and (c).

III. Electromagnetic Analysis and Comparison

For the sake of clear analysis, the proposed structure will be compared with the conventional closed-core and open-core transformers. The material of the transformer core is PC44 and the air gap of the open-core transformer and NMRS-based transformer is designed as 0.6 mm. The *B–H* relationship of PC44 can maintain linear if the magnetic induction intensity *B* is no more than 0.4 T. The magnetizing current of the open-core, the closed-core, and the NMRS-based transformers are 0.4 A, 3.8 A, and 0.8 A, respectively. Using the current source with corresponding magnetizing currents as the excitation, the core magnetic induction intensity *B* of those three transformers is approximately equal, which is shown in Fig. 7(a)–(c).

The impacts of different dc biases current on magnetic induction intensity *B* of the core are demonstrated in Fig. 7(d)–(l). The magnetic core of the closed-core transformer is approaching saturation when the dc bias reaches 0.2 A, as shown in Fig. 7(d). If the dc bias current is larger than 0.2 A, the magnetic core reaches the deep saturation region and the performance of the transformer will decrease sharply.

The open-core and the NMRS-based transformer indicate a strong withstand dc bias capability, which can withstand the 2-A dc bias current shown in Fig. 7(j). Even when the dc bias current of the NMRS-based transformer reaches 2 A, its saturation degree (0.36 T) is still far less than the closed-core transformer with a 0.2-A dc bias current (0.39 T).

Besides, as shown in Fig. 7(j) and (l), although the saturation degree of the NMRS-based transformer is more serious than that of the open-core transformer with the same dc bias, the magnetizing current of the former is still far less than that of former. It will bring the NMRS-based transformer a higher efficiency compared to the generalized open-core transformer.

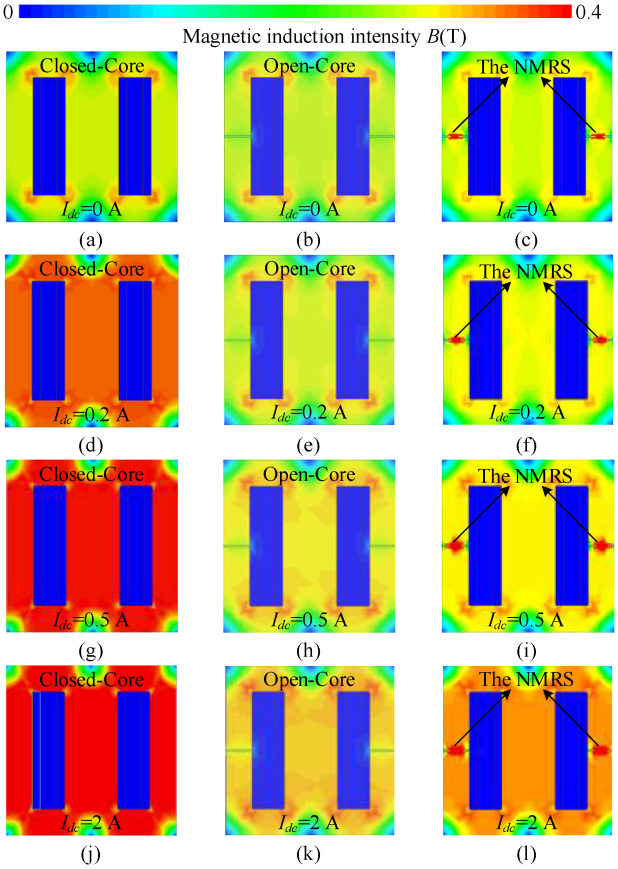

Fig. 7. Electromagnetic analysis of the closed-core transformer (type A), open-core transformer (type B), and the NMRS-based transformer (type C) under dc bias. (a) Type A without dc bias. (b) Type B without dc bias. (c) Type C without dc bias. (d) Type A with 0.2 A. (e) Type B with 0.2 A. (f) Type C with 0.2 A. (g) Type A with 0.5 A. (h) Type B with 0.5 A. (i) Type C with 0.5 A. (j) Type A with 2 A. (k) Type B with 2 A, and (l) Type C with 2 A.

Based on the abovementioned analysis, the proposed NMRS-based transformer provides a strong withstanding dc bias capability as the open-core transformer. Detailed efficiency verification will be conducted in the next section.

IV. Experimental Verification

The experimental verification test bed consists of the signal generator (SDG 1032X), power amplifier (AE Techron 7224), dc source (MCH-K605D), oscilloscope (ZDS3024), load, and the NMRS-based transformers, which are shown in Fig.8. The NMRS-based transformer, magnetic core, and NMRS are shown in Fig. 9.

For conducting a detailed comparison, the experimental results with sinusoidal excitation and square wave excitation are given to verify the operation condition in ac–dc matrix converters [12] and DAB applications [10].

A. Normal Operating Condition Analysis

The no-load (magnetizing) current is to generate the flux in the magnetic core to transfer the power from the primary side

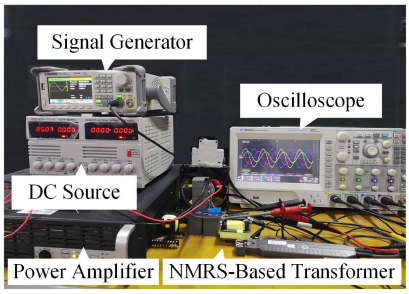

Fig. 8. Experimental platform of the transformer.

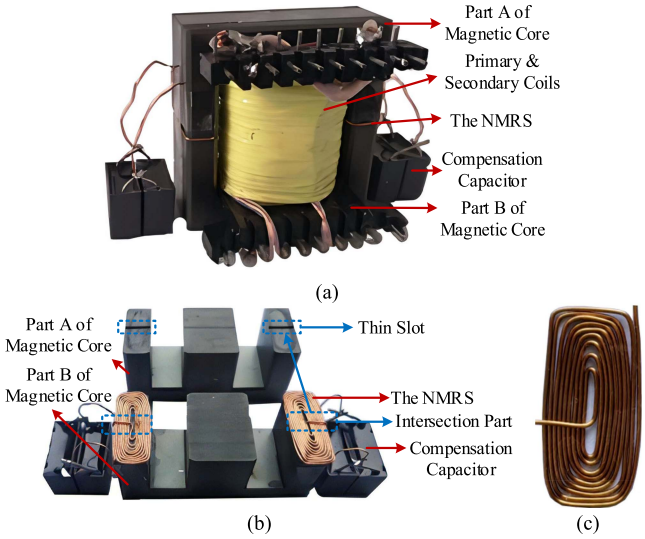

Fig. 9. Prototype of the NMRS and NMRS-based transformer. (a) NMRS-based transformer. (b) Magnetic core. (c) NMRS.

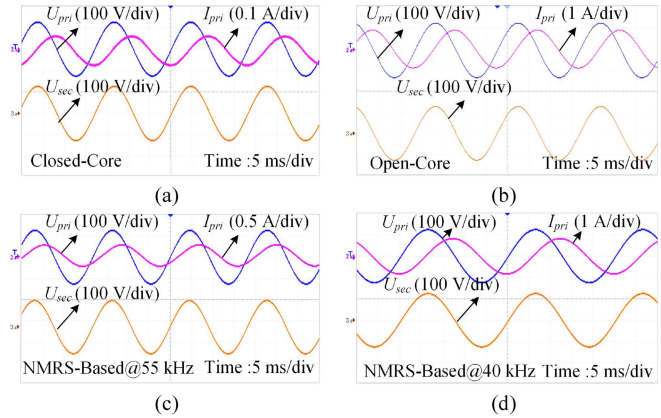

Fig. 10. Experimental results of no-load operating condition with sinusoidal excitation. (a) Closed-core transformer. (b) Open-core transformer. (c) NMRS-based transformer at the negative magnetic reluctance region (55 kHz). (d) NMRS-based transformer out of the negative magnetic reluctance frequency region (40 kHz).

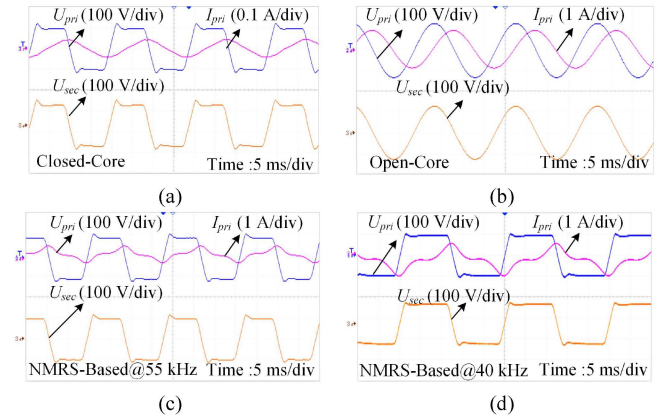

Fig. 11. Experimental results of no-load operating condition with square wave excitation. (a) Closed-core transformer. (b) Open-core transformer. (c) NMRS-based transformer at the negative magnetic reluctance region (55 kHz). (d) NMRS-based transformer out of the negative magnetic reluctance frequency region (40 kHz).

to the secondary side of the transformer [37]. The primary coil current consists of the magnetic current and the load current, shown as

$$\boldsymbol{i}_{\mathbf{pri}} = \boldsymbol{i}_{\mathbf{mag}} + \boldsymbol{i}_{\mathbf{pri\_load}} \tag{14}$$

where $\boldsymbol{i}_{\mathbf{pri}}$, $\boldsymbol{i}_{\mathbf{mag}}$, and $\boldsymbol{i}_{\mathbf{pri\_load}}$ are the current vector of the primary coil, magnetizing current vector, and the current vector caused by the load.

The efficiency of the transformer is defined as

$$\eta = \frac{U_{\text{sec}} I_{\text{sec}} \cos(\theta_{\text{sec}})}{U_{\text{pri}} I_{\text{pri}} \cos(\theta_{\text{pri}})} = \frac{U_{\text{sec}} I_{\text{sec}} \cos(\theta_{\text{sec}})}{U_{\text{pri}} (I_{\text{pri\_load}} + I_{\text{mag}}) \cos(\theta_{\text{pri}})} \tag{15}$$

where U_{sec} , U_{pri}, I_{sec}, and I_{pri} are the effective value of the output and input voltage as well as that of the output and input current. θ_{sec} and θ_{pri} are the phase difference between the output and input voltage and current.

If the load is resistive, the magnetizing current will only reduce the power factor of the transformer. However, in most of the applications, the load is inductive, which improves the phase difference θ_{pri}. Hence, with the inductive load, as shown in (11), the efficiency of the transformer is inversely proportional to the magnetizing current I_{mag}. Theoretically, a lower magnetizing current will lead to a high power transfer efficiency and power factor. I_{mag} is stable with a fixed input voltage.

Under the no-load condition, the primary current only consists of the magnetizing current I_{mag}. Hence, by evaluating I_{mag} , the performance of the transformer under on-load conditions can be obtained.

The magnetizing current of the open-core and closed-core transformer, as well as the NMRS-based transformer at the designed frequency, is shown in Fig. 10. Besides, a contrast experiment of the NMRS-based transformer is also conducted under 40 kHz, which is beyond the negative magnetic reluctance operating frequency region. As shown in Fig. 10, the NMRS reduces the magnetizing current compared to the open-core transformer from 689 to 166 mA.

Apart from the sinusoidal excitation, the magnetizing current induced by the square wave excitation is indicated in Fig. 11. The magnetizing currents of the closed-core and open-core transformers are 57.5 and 665 mA, respectively, whereas the magnetizing currents, at the negative magnetic reluctance region

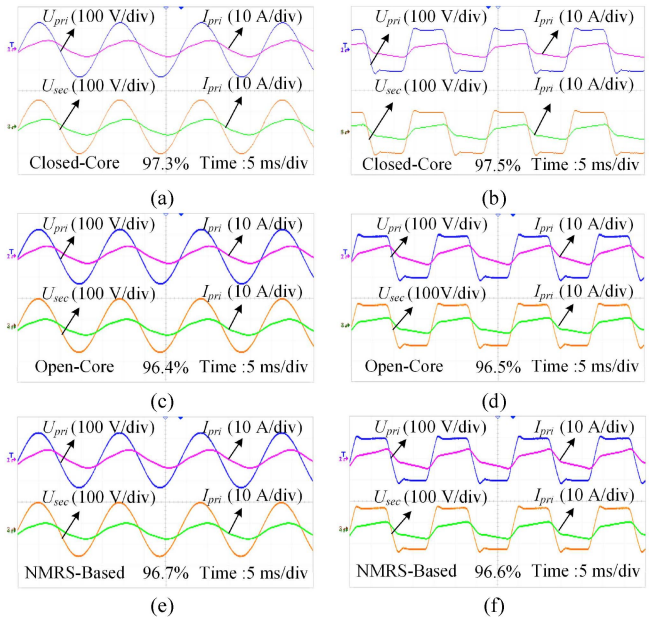

Fig. 12. Experimental results of 200 W. (a) Closed-core with sinusoidal excitation. (b) Closed-core with square wave excitation (c) Open-core with sinusoidal excitation. (d) Open-core with square wave excitation. (e) NMRS-based with sinusoidal excitation. (f) NMRS-based with square wave excitation.

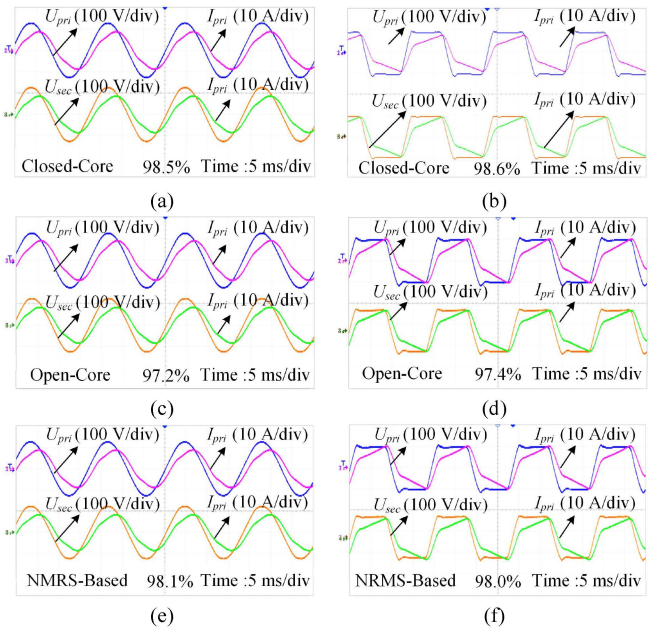

Fig. 13. Experimental results of 500 W. (a) Closed-core with sinusoidal excitation. (b) Closed-core with square wave excitation. (c) Open-core with sinusoidal excitation. (d) Open-core with square wave excitation. (e) NMRS-based with sinusoidal excitation. (f) NMRS-based with square wave excitation.

and out of that region of the NMRS-based transformer, are 218 and 733 mA, respectively. The results indicate an identical trend with the sinusoidal excitation in Fig. 10.

The 200- and 500-W on-load experimental verifications of those three transformers with sinusoidal and square wave excitation are shown in Figs. 12 and 13, respectively. At the power level

TABLE III
PERFORMANCE OF THE TRANSFORMERS UNDER NO DC BIAS

Type	Closed-Core	Open-Core	NMRS-Based
magnetizing Current (sin)	43 mA	689 mA	166 mA
magnetizing Current (square)	57.5 mA	733 mA	218 mA
200W efficiency(sin)	97.3%	96.4%	96.7%
200W efficiency(square)	97.5%	96.5%	96.6%
350W efficiency(sin)	98.2%	96.6%	97.4%
350W efficiency(square)	98.2%	96.7%	97.1%
500W efficiency(sin)	98.5%	97.2%	98.1%
500W efficiency(square)	98.6%	97.4%	98.0%

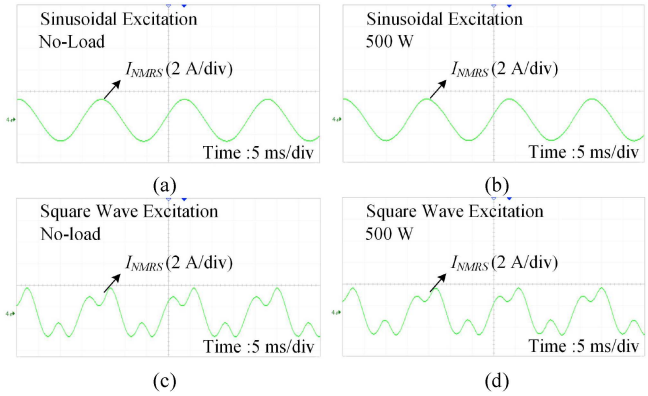

Fig. 14. Current through the NMRS under different excitation and power level. (a) 90-V sinusoidal excitation and no load. (b) 90-V sinusoidal excitation and 500 W. (c) 90-V square wave excitation and no load. (d) 90-V square wave excitation and 500 W.

of 200 W in Fig. 12, the efficiency of the closed-core transformer is 97.3% with sinusoidal excitation and 97.5% with square wave excitation, respectively. The attainable efficiencies are the highest among those aforementioned three transformers. The efficiencies of the open-core and the NMRS-based transformer are 96.4% and 96.7% with sinusoidal excitation and 96.5% and 96.6% with square wave excitation. The efficiency improvement is not significant under the condition of the light load. If the load gets heavy, the efficiency promotion of the NMRS will be apparent, as shown in Fig. 13.

As shown in Fig. 13, under the power level of 500 W, the efficiency promotion of the NMRS-based transformer reaches 0.9% with sinusoidal excitation and 0.6% with square wave excitation, respectively, which is significantly larger than that under 200 W. To evaluate the performance of the NMRS-based transformer better, the 200-, 350-, and 500-W experiments are conducted and the corresponding results are given in Table III. As shown in Table III, the efficiency NMRS-based transformer is larger than that of the open-core transformer and close to that of the closed-core transformer.

The current waveforms through the NMRS with the sinusoidal excitation and square excitation are given in Fig. 14.

The variation of the current through NMRS with 90-V excitation under different power levels is small. The variation current is from 1.337 to 1.384 A with sinusoidal excitation as well as from 1.444 to 1.479 A with square wave excitation, varying from the load condition.

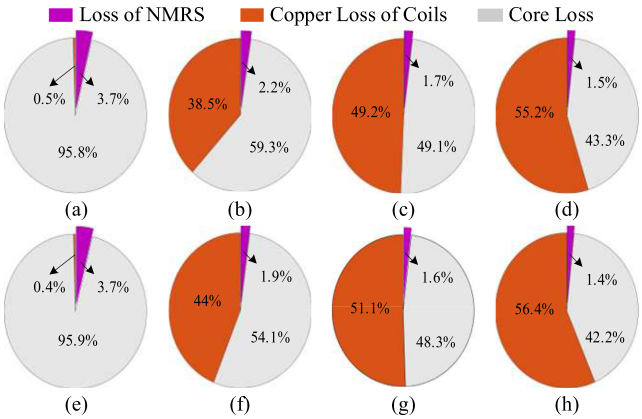

Fig. 15. Loss distribution of the NMRS-based transformer. (a) Sinusoidal and no load. (b) Sinusoidal and 200 W. (c) Sinusoidal and 350 W. (d) Sinusoidal and 500 W. (e) Square wave and no load. (f) Square wave and 200 W. (g) Square wave and 350 W. (h) Square wave and 500 W.

Based on the data indicated in Figs. 12–14, the loss distributions of the transformers are given in Fig. 15. As shown in Fig. 15, the proportion of the loss caused by the NMRS is decreased with the increase of the power level with both the square wave and sinusoidal excitation. Under on-load operating conditions, the share of the NMRS loss is not larger than 2.2% compared to the total loss.

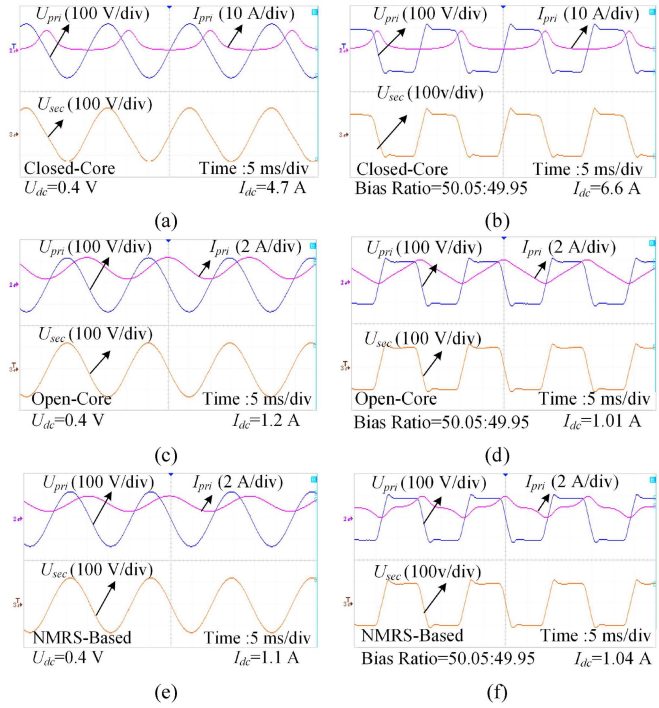

Fig. 16. Experimental results of transformers with different dc. (a) Closed-core transformer with 4.7-A bias. (b) Closed-core transformer with 6.6-A bias. (c) Open-core transformer with 1.2-A bias. (d) Open-core transformer with 1.01-A bias. (e) NMRS-based transformer with 1.1-A bias. (f) NMRS-based transformer with 1.04 A bias.

B. DC Bias Operating Condition Analysis

In this part, the power experiment and inductance measurement experiment will be conducted to verify the performance of open-core, closed-core, and NMRS-based transformers under different dc biases.

As for the first method, the experiment platform is shown in Fig. 8. For conducting an effective comparison, the source of the experimental platform is selected as the voltage source with both sinusoidal excitation to verify the operation condition in the ac–dc matrix converter and square waves excitation to verify that in DAB applications, respectively. The dc bias current is achieved via modifying the dc bias voltage of sinusoidal excitation and duty cycles of square wave excitation.

Experimental results regarding the dc bias are given in Fig. 16. As shown in Fig. 16(a), (c), and (e), a dc bias voltage of 0.4 V will lead to a 4.7-A bias current of the closed-core transformer with the sinusoidal excitation. Correspondingly, the same dc bias voltage will only cause a 1.2- and 1.1-A bias current of the open-core and NMRS-based transformer. This trend can be also found in the transformers with square wave excitation, which is shown in Fig. 16(b), (d), and (f).

The bias ratio is the proportion between the positive and negative parts of the square wave. With the bias ratio of 50.05:49.95, the dc bias currents of the closed-core, open-core, and NMRS-based transformers are 6.6, 1.01, and 1.04 A, respectively. It is noticeable that the open-core and the NMRS can significantly reduce the dc bias current caused by the asymmetrical excitation, indicating a strong anti-dc bias capability.

However, the withstand dc bias capability varies from the load condition, hence, Apart from the abovementioned method, observing the inductance L is also a widely used solution to evaluate the withstand dc bias capability.

The inductance L of the primary coil and secondary coil is another parameter to verify the withstand dc bias capability of the transformer, which can be verified as follows.

Based on (3), the relationship between inductance and the flux can be expressed as follows:

$$\phi = Li = BS = \frac{Ni}{R_m} \tag{16}$$

where ϕ, B, and S are the flux, magnetic induction intensity, and the cross area of the magnetic core, whereas L and i are the inductance and the current of the coil. R_m is the overall magnetic reluctance of the transformer. The maximum magnetic induction intensity B of the magnetic core material, PC 44, is 0.4 T. The relationship between the magnetic field intensity H and magnetic induction intensity B is defined as

$$B = \mu H = \mu \frac{Ni}{l} \tag{17}$$

where l is the equivalent length of the magnetic core.

Based on (16)–(8), the inductance L of the coil is expressed by the induction intensity B and magnetic field intensity H, shown as follows:

$$L = \frac{NS}{l} \frac{B}{H} = \frac{N^2}{R_m}. \tag{18}$$

According to (18), the inductance L can be regarded as the slope of the B–H (B–i) relationship shown in Fig. 3. The

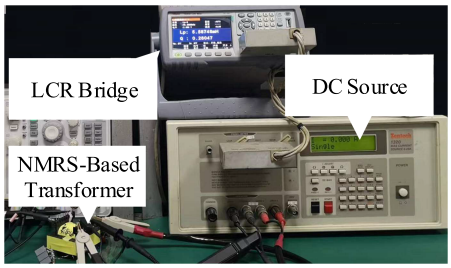

Fig. 17. Inductance measurement platform.

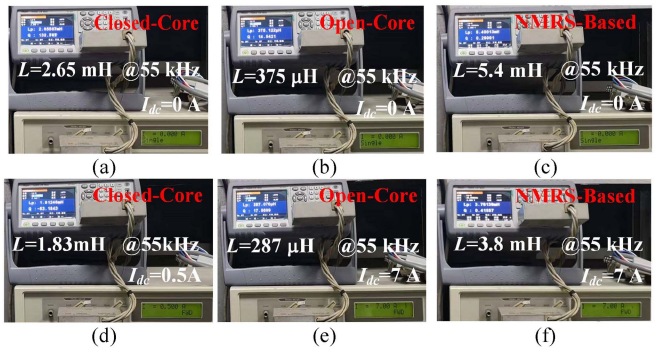

Fig. 18. Inductance of coil with/without dc bias current at different frequencies. (a) Closed-core without dc bias at 55 kHz. (b) Open-core without dc bias at 55 kHz. (c) NRMS-based without dc bias at 55 kHz. (d) Closed-core with dc bias of 0.5 A at 55 kHz. (e) Open-core with dc bias of 7 A at 55 kHz. (f) NRMS-based without dc bias of 7 A at 55 kHz.

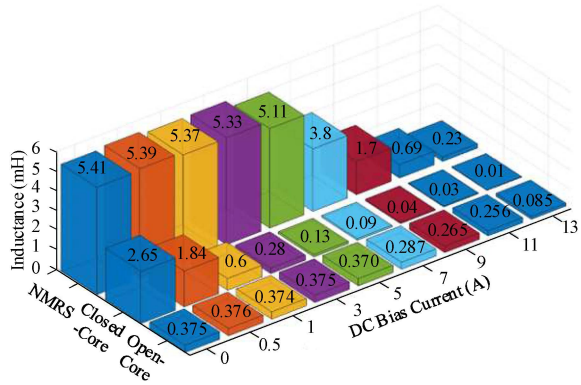

Fig. 19. Relationships between the inductance, dc bias current, and type of transformers under 55 kHz.

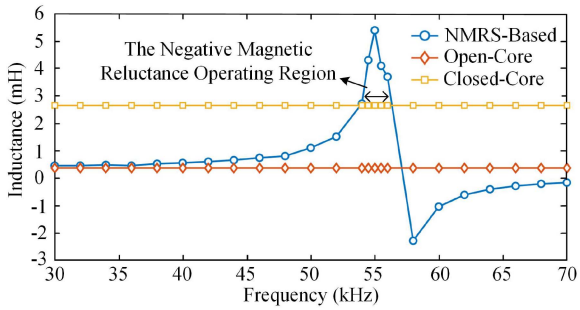

Fig. 20. Frequency versus inductance of the primary coil of transformers.

magnetic field intensity H will increase with the rise of the dc bias current. Under the unsaturation region, the B–H relationship is stable, making the inductance L fixed. However, under the saturation region, induction intensity B cannot keep increasing with the rising magnetic field intensity H. The slope of the B–H relationship and the inductance L will sharply decrease. Correspondingly, the dc bias current will distort the flux in a semicircle and lead to saturation of the transformer. Hence, by observing the inductance of coils, the withstand dc bias capability can be demonstrated.

The experimental platform of inductance measurement is shown in Fig. 17, including a dc source, an *LCR* bridge, and a transformer. The experimental results and comparison are shown in Figs. 18 and 19, respectively.

As shown in Fig. 18(a)–(c), the inductance L of the NMRS-based transformer is the highest at 55 kHz, for the NMRS shows a negative magnetic reluctance at that frequency. Figs. 18(d)–(f) demonstrates the impact of dc bias on the inductances L of the closed-core, open-core, and NMRS-based transformers when their inductances have a 30% reduction.

The detailed results of inductance L measurement with different dc bias currents are shown in Fig. 19. The closed-core transformer will enter into the saturation region when the dc bias current is larger than 0.5 A, whereas the open-core and the NMRS-based transformer can maintain unsaturated unless the dc bias current reaches 4.5 A. Besides, the coils of NMRS-based transformer have an overall highest inductance, which is much larger than that of the open-core transformer. It will bring a lower magnetizing current and higher efficiency to the transformer. Furthermore, the proposed structure can withstand more than the dc bias of 4 A, whereas the open-core transformer cannot operate normally with that of 0.5 A.

C. NMRS Property Analysis

The negative magnetic reluctance and harmonic suppression properties are verified via inductance measurement. Based on the inductance value of the open-core and closed-core transformer, the inductance of the NMRS-based transformer can be used to evaluate the magnetic reluctance of the NMRS. The frequency versus inductance of the transformer coil is shown in Fig. 20.

Based on the structures of closed-core, open-core, and NMRS-based transformers, the overall magnetic reluctance R_m of them is defined as follows:

$$R_m = \frac{l}{\mu A} \approx \begin{cases} R_{\text{core}} + R_{\text{Air}}, & \text{Open Core} \\ R_{\text{core}}, & \text{Closed Core} \\ R_{\text{core}} + R_{\text{NMRS}}, & \text{NMRS Based} \end{cases} \tag{19}$$

where R_{core}, R_{air}, and R_{NMRS} are the magnetic reluctance of the magnetic core of the transformer, air, and the proposed NMRS, respectively.

Based on (18) and (19), the inductance L of a coil is inversely proportional to the overall magnetic reluctance. For the open-core and closed-core transformers, the magnetic reluctance R_m will not change under frequency variation while that of

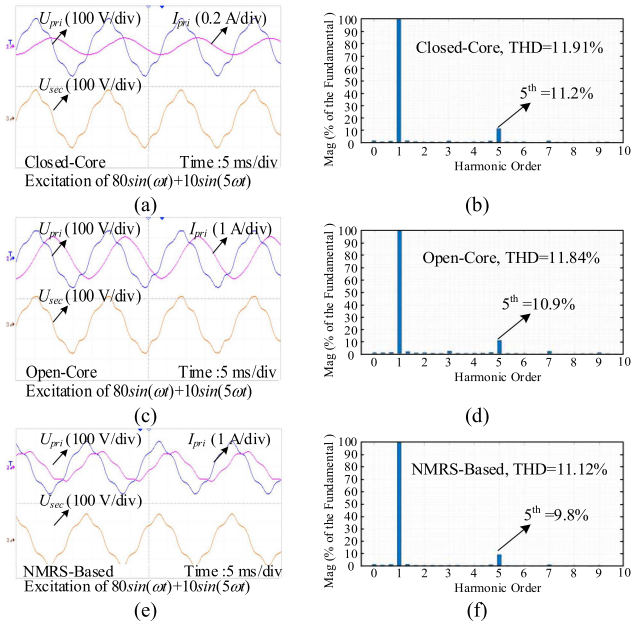

Fig. 21. Harmonic injection experiments for transformers. (a) Closed-core transformer. (b) THD of the closed-core secondary voltage. (c) Open-core transformer. (d) THD of the open-core secondary voltage. (e) NMRS-based transformer. (f) THD of the NMRS-based secondary voltage.

the NMRS-based transformer will be varied with frequency. Correspondingly, the negative magnetic reluctance of the NMRS can be obtained when its inductance is larger than that of the closed-core transformer.

Hence, the best relative permeability μ_{NMRS} can be obtained with a maximum positive inductance and calculated by the magnetic reluctance of those transformers, which is shown as

$$\mu_{\text{NMRS}} = \frac{R_{\text{air}}}{R_{\text{NMRS}}}\ \mu_0 = -15.52 \tag{20}$$

where μ_{NMRS} and μ_0 are the relative permeability of NMRS and air, respectively.

For evaluating the effect of the proposed NMRS on harmonics, harmonic injection experiment results are given. The input voltage of the transformers is set as $80\sin(\omega t)+10\sin(5\omega t)$, where ω is the corresponding radian frequency of the operating frequency 55 kHz. By injecting the high-order harmonics, the harmonics optimized effectiveness of the NMRS can be verified by comparing the total harmonic distortion (THD) of open-core, closed-core, and NMRS-based transformers. The relevant results are shown in Fig. 21.

As shown in Fig. 21, the fifth-harmonic component of the NMRS-based transformer is lower than that of the open-core and closed-core transformers, indicating the harmonic property of the proposed design. The fifth-harmonic contents of the closed-core, open-core, and NMRS-based transformer are 11.2%, 10.9%, and 9.8%, respectively.

V. Conclusion

This article proposes a passive NMRS to improve the efficiency and withstand the dc bias capability of the kHz transformer. The equivalent magnetic circuit of the transformer, the mathematical model of the NMRS, and the theoretical feasibility of the overall system are established and verified.

The negative magnetic reluctance and harmonic property of the proposed NMRS are verified by inductance measurement and harmonic injection experiments.

The normal operating conditions of the NMRS-based transformer and contrast models with both sinusoidal and square wave excitation are conducted. When sinusoidal excitation and square wave excitation are enabled, the proposed structure effectively reduces the magnetizing current from 689/733 mA to 166/218 mA. Meanwhile, it improves the efficiency of the transformer by 0.9/0.6% under the power level of 500 W compared with the open-core transformer.

The dc bias experiment results demonstrate the withstanding dc bias capability of the proposed structure. If sinusoidal excitation and square wave excitation are activated, with the same dc bias voltage, the NMRS-based transformer can reduce the dc bias current from 6.4/4.7 A to 1.1/1.04 A compared to the closed-core transformer.

Strong dc bias withstanding capability for open-core transformers and high efficiency for closed-core transformers are simultaneously presented in the proposed design, which confirms its superiority in industrial application.

References

[1] M. Ekhtiari, T. Andersen, M. A. E. Andersen, and Z. Zhang, "Dynamic optimum dead time in piezoelectric transformer-based switch-mode power supplies," *IEEE Trans. Power Electron.*, vol. 32, no. 1, pp. 783–793, Jan. 2017.

[2] Y. Li et al., "An inductively filtered multiwinding rectifier transformer and its application in industrial DC power supply system," *IEEE Trans. Ind. Electron.*, vol. 63, no. 7, pp. 3987–3997, Jul. 2016.

[3] G. Li, J. Xia, K. Wang, Y. Deng, X. He, and Y. Wang, "Hybrid modulation of parallel-series *LLC* resonant converter and phase shift full-bridge converter for a dual-output DC–DC converter," *IEEE J. Emerg. Sel. Topics Power Electron.*, vol. 7, no. 2, pp. 833–842, Jun. 2019.

[4] C.-Y. Lim, Y. Jeong, and G.-W. Moon, "Phase-shifted full-bridge DC–DC converter with high efficiency and high power density using center-tapped clamp circuit for battery charging in electric vehicles," *IEEE Trans. Power Electron.*, vol. 34, no. 11, pp. 10945–10959, Nov. 2019.

[5] A. K. Paul, "Efficacy of STC in high frequency full-bridge DC-DC converter," *IEEE J. Emerg. Sel. Topics Ind. Electron.*, to be published, doi: 10.1109/JESTIE.2022.3165992.

[6] S. Baek and S. Bhattacharya, "Analytical modeling and implementation of a coaxially wound transformer with integrated filter inductance for isolated soft-switching DC–DC converters," *IEEE Trans. Ind. Electron.*, vol. 65, no. 3, pp. 2245–2255, Mar. 2018.

[7] J. Zhang, J. Liu, S. Zhong, J. Yang, N. Zhao, and T. Q. Zheng, "A power electronic traction transformer configuration with low-voltage IGBTs for onboard traction application," *IEEE Trans. Power Electron.*, vol. 34, no. 9, pp. 8453–8467, Sep. 2019.

[8] N. Zhao, J. Liu, Y. Ai, J. Yang, J. Zhang, and X. You, "Power-linked predictive control strategy for power electronic traction transformer," *IEEE Trans. Power Electron.*, vol. 35, no. 6, pp. 6559–6571, Jun. 2020.

[9] J. Zhang, J. Liu, J. Yang, N. Zhao, Y. Wang, and T. Q. Zheng, "A modified DC power electronic transformer based on series connection of full-bridge converters," *IEEE Trans. Power Electron.*, vol. 34, no. 3, pp. 2119–2133, Mar. 2019.

[10] A. Mercier, K. Zehani, G. Chaplier, A. Pasko, V. Loyau, and F. Mazaleyrat, "Spark plasma sintering co-sintered monolithic transformers for power electronics," *IEEE Trans. Magn.*, vol. 52, no. 5, May 2016, Art. no. 8400404.

[11] G. Ortiz, H. Uemura, D. Bortis, J. W. Kolar, and O. Apeldoorn, "Modeling of soft-switching losses of IGBTs in high-power high-efficiency dual-active-bridge DC/DC converters," *IEEE Trans. Electron Devices*, vol. 60, no. 2, pp. 587–597, Feb. 2013.

[12] F. Krismer and J. W. Kolar, "Efficiency-optimized high-current dual active bridge converter for automotive applications," *IEEE Trans. Ind. Electron.*, vol. 59, no. 7, pp. 2745–2760, Jul. 2012.
[13] S. Bal, D. B. Yelaverthi, A. K. Rathore, and D. Srinivasan, "Improved modulation strategy using dual phase shift modulation for active commutated current-fed dual active bridge," *IEEE Trans. Power Electron.*, vol. 33, no. 9, pp. 7359–7375, Sep. 2018.
[14] J. Hu, S. Cui, and R. W. De Doncker, "Natural boundary transition and inherent dynamic control of a hybrid-mode-modulated dual-active-bridge converter," *IEEE Trans. Power Electron.*, vol. 37, no. 4, pp. 3865–3877, Apr. 2022.
[15] U. Nasir, A. Costabeber, M. Rivera, P. Wheeler, and J. Clare, "A leakage-inductance-tolerant commutation strategy for isolated AC/AC converters," *IEEE J. Emerg. Sel. Topics Power Electron.*, vol. 7, no. 1, pp. 467–479, Mar. 2019.
[16] W. Hu, Y. Xie, Y. Guan, Z. Wang, Z. Zhang, and J. Xu, "A novel volt-second self-balancing SVPWM scheme to eliminate steady-state DC bias for a three-phase isolated AC–DC matrix converter," *IEEE Trans. Power Electron.*, vol. 35, no. 11, pp. 11518–11532, Nov. 2020.
[17] G. Buticchi and E. Lorenzani, "Detection method of the DC bias in distribution power transformers," *IEEE Trans. Ind. Electron.*, vol. 60, no. 8, pp. 3539–3549, Aug. 2013.
[18] Z. Zhao et al., "Measurements and calculation of core-based *B-H* curve and magnetizing current in DC-biased transformers," *IEEE Trans. Appl. Supercond.*, vol. 20, no. 3, pp. 1131–1134, Jun. 2010.
[19] X. Chen, Z. Wang, and B. Wang, "Research on dynamic magnetic flux measurement under DC-biased magnetization by the type-C transducer," *IEEE Trans. Magn.*, vol. 51, no. 11, Nov. 2015, Art. no. 6101304.
[20] L. Shu, W. Chen, and Z. Song, "Prediction method of DC bias in DC-DC dual-active-bridge converter," *CPSS Trans. Power Electron. Appl.*, vol. 4, no. 2, pp. 152–162, Jun. 2019.
[21] O. Biro, G. Buchgraber, G. Leber, and K. Preis, "Prediction of magnetizing current wave-forms in a three-phase power transformer under DC bias," *IEEE Trans. Magn.*, vol. 44, no. 6, pp. 1554–1557, Jun. 2008.
[22] K. Sakuma, K. Shigeuchi, J. Xu, N. Shimosato, and Y. Sato, "Decoupling control method for eliminating DC bias flux of high frequency transformer in a bidirectional isolated AC/DC converter," in *Proc. Int. Power Electron. Conf.*, 2018, pp. 3522–3527.
[23] Z. Chen, H. Li, L. Liu, L. Xiang, and B. Bai, "DC bias treatment of hybrid type transformer based on magnetic flux modulation mechanism," *IEEE Trans. Magn.*, vol. 55, no. 6, Jun. 2019, Art. no. 1700204.
[24] B. Bai, Z. Chen, and D. Chen, "DC bias elimination and integrated magnetic technology in power transformer," *IEEE Trans. Magn.*, vol. 51, no. 11, Nov. 2015, Art. no. 8401304.
[25] X. Chen, Z. Wang, and B. Wang, "Research on dynamic magnetic flux measurement under DC-biased magnetization by the type-c transducer," *IEEE Trans. Magn.*, vol. 51, no. 11, Nov. 2015, Art. no. 6101304.
[26] P. Yao, X. Jiang, P. Xue, S. Ji, and F. Wang, "Flux balancing control of ungapped nanocrystalline core-based transformer in dual active bridge converters," *IEEE Trans. Power Electron.*, vol. 35, no. 11, pp. 11463–11474, Nov. 2020.
[27] Z. Xie et al., "Advanced DC bias suppression strategy based on finite DC blocking devices," *IEEE Trans. Power Del.*, vol. 32, no. 6, pp. 2500–2509, Dec. 2017.
[28] P. Yao, X. Jiang, P. Xue, S. Li, S. Lu, and F. Wang, "Design optimization of medium-frequency transformer for DAB converters with DC bias capacity," *IEEE J. Emerg. Sel. Topics Power Electron.*, vol. 9, no. 4, pp. 5043–5054, Aug. 2021.
[29] H. Wang, W. Wang, X. Chen, Q. Li, and Z. Zhang, "Analysis and design of kHz-metamaterial for wireless power transfer," *IEEE Trans. Magn.*, vol. 56, no. 8, Aug. 2020, Art. no. 6703215.
[30] J. Zhou, P. Zhang, J. Han, L. Li, and Y. Huang, "Metamaterials and metasurfaces for wireless power transfer and energy harvesting," *Proc. IEEE*, vol. 110, no. 1, pp. 31–55, Jan. 2022.
[31] Z. Zhang, H. Pang, A. Georgiadis, and C. Cecati, "Wireless power transfer—An overview," *IEEE Trans. Ind. Electron.*, vol. 66, no. 2, pp. 1044–1058, Feb. 2019.
[32] R. Das, A. Basir, and H. Yoo, "A metamaterial-coupled wireless power transfer system based on cubic high-dielectric resonators," *IEEE Trans. Ind. Electron.*, vol. 66, no. 9, pp. 7397–7406, Sep. 2019.
[33] C. Lu et al., "Investigation of negative and near-zero permeability metamaterials for increased efficiency and reduced electromagnetic field leakage in a wireless power transfer system," *IEEE Trans. Electromagn. Compat.*, vol. 61, no. 5, pp. 1438–1446, Oct. 2019.
[34] H. Wang, W. Wang, X. Chen, Q. Li, and Z. Zhang, "Analysis and design of kHz-metamaterial for wireless power transfer," *IEEE Trans. Magn.*, vol. 56, no. 8, Aug. 2020, Art. no. 6703215.
[35] W. Adepoju et al., "Critical review of recent advancement in metamaterial design for wireless power transfer," *IEEE Access*, vol. 10, pp. 42699–42726, 2022.
[36] Z. Gong and S. Yang, "One-dimensional stacking miniaturized low-frequency metamaterial bulk for near-field applications," *J. Appl. Phys.*, vol. 127, no. 11, 2020, Art. no. 114901.
[37] G. Delette, U. Soupremanien, and S. Loudot, "Thermal management design of transformers for dual active bridge power converters," *IEEE Trans. Power Electron.*, vol. 37, no. 7, pp. 8301–8309, Jul. 2022.

Yuanxi Chen received the B.Eng. and M.Eng. degrees from Huaqiao University, Xiamen, China, in 2015 and 2018, respectively. He is currently working toward the Ph.D. degree in electrical engineering with The Hong Kong Polytechnic University, Hong Kong, SAR, China.

His research interests include electrical machine design, electromagnetic metamaterial, and transformer and wireless power transmission.

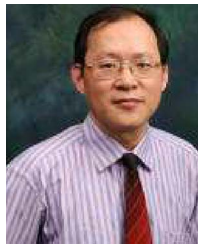

Weinong Fu received the Ph.D. degree from The Hong Kong Polytechnic University (PolyU), Hong Kong, SAR, China, in 1999.

He is currently a Professor with Shenzhen Institutes of Advanced Technology, Chinese Academy of Sciences, Beijing, China. For 13 years, he was an Associate Professor and a Full Professor with PolyU. He was a Key Developer with Ansoft Corporation, Pittsburgh, PA, USA. He has about seven years of working experience with Ansoft, focusing on the development of commercial software Maxwell. His research interests include computational electromagnetics, optimal design of electric devices, applied electromagnetics, and novel electric machines. He has made many contributions to the theory and application of electromagnetic field computation and electric device designs, including the publication of more than 250 refereed journal papers.

Hongjian Lin (Member, IEEE) received the Ph.D. degree in electrical engineering from Southwest Jiaotong University, Chengdu, China, in 2021.

From 2019 to 2020, he was a Visiting Researcher with the School of Electrical and Computer Engineering, Georgia Institute of Technology, Atlanta, GA, USA. He is currently a Postdoc Research Associate with the Department of Electrical Engineering, The Hong Kong Polytechnic University, Hong Kong, SAR, China. His research interests include electrical machines and drives, electric traction supply systems, and modulation and control technologies of multilevel converters in solid-state transformers.

Shuangxia Niu (Senior Member, IEEE) received the B.Sc. and M.Sc. degrees from Tianjin University, Tianjin, China, and the Ph.D. degree from the University of Hong Kong, Hong Kong, SAR, China, all in electrical engineering.

She is currently an Associate Professor with the Department of Electrical Engineering, The Hong Kong Polytechnic University. She authored or coauthored more than 100 papers in leading journals.

Prof. Niu is currently an Associate Editor for the IEEE JOURNAL OF EMERGING AND SELECTED TOPICS IN POWER ELECTRONICS.